Title

Studies on the phase diagram of Pb–Fe–O system and standard molar Gibbs energy of formation of ‘PbFe5O8.5’ and Pb2Fe2O5

Journal

Journal of Nuclear Materials, 426

Author

Sahu, Sulata Kumari

Publication Date

2012

Peer reviewed

Journal of Nuclear Materials 426 (2012) 214–222

Contents lists available at SciVerse ScienceDirect

Journal of Nuclear Materials

journal homepage: www.elsevier.com/locate/jnucmat

Studies on the phase diagram of Pb–Fe–O system and standard molar Gibbs energy of formation of '$PbFe_5O_{8.5}$' and $Pb_2Fe_2O_5$

Sulata Kumari Sahu, Rajesh Ganesan, T. Gnanasekaran *

Liquid Metals and Structural Chemistry Division, Chemistry Group, Indira Gandhi Centre for Atomic Research, Kalpakkam 603 102, India

ARTICLE INFO

Article history:
Received 2 December 2011
Accepted 17 March 2012
Available online 29 March 2012

ABSTRACT

Partial phase diagram of Pb–Fe–O system has been established by phase equilibration studies over a wide temperature range coupled with high temperature solid electrolyte based emf cells. Ternary oxides are found to coexist with liquid lead only at temperatures above 900 K. At temperatures below 900 K, iron oxides coexist with liquid lead.

Standard molar Gibbs energy of formation of ternary oxides '$PbFe_5O_{8.5}$' and $Pb_2Fe_2O_5$ were determined by measuring equilibrium oxygen partial pressures over relevant phase fields using emf cells and are given by the following expressions:

$$\Delta_f G^o_m \text{ '}PbFe_5O_{8.5}\text{'} \pm 1.0(\text{kJ mol}^{-1}) = -2208.1 + 0.6677(T/\text{K}) \quad (917 \leqslant T/\text{K} \leqslant 1117)$$

$$\Delta_f G^o_m \; Pb_2Fe_2O_5 \pm 0.8(\text{kJ mol}^{-1}) = -1178.4 + 0.3724(T/\text{K}) \quad (1050 \leqslant T/\text{K} \leqslant 1131)$$

.

1. Introduction

Liquid lead and Lead–Bismuth Eutectic (LBE) are the candidate coolants for Generation IV nuclear reactors and are also considered as spallation neutron targets as well as coolants in accelerator driven systems because of their favorable thermal, physical and chemical properties [1]. However, they are highly corrosive towards the structural steels. One of the approaches to minimize this corrosion is to control the dissolved oxygen content in these liquid metals so as to form a protective oxide film on the steel surface [2–6]. Formation of a protective oxide film on the surface of the steel reduces direct dissolution of the steel components owing to the low diffusion coefficients of the alloying components through the oxide film [7,8]. To understand the composition of the protective oxide film and its stability, a detailed knowledge on the phase diagrams of Pb–M–O and Bi–M–O systems (M = alloying components of steels) as well as the thermochemical data on ternary oxides formed in these systems is essential. A systematic study of Pb–M–O systems (M = Fe, Cr) is being carried out at the authors' laboratory. Although many of the ternary compounds involved in Pb–M–O systems and pseudo binary diagrams of $PbO–CrO_3$ and $PbO–Fe_2O_3$ systems have been reported, their equilibrium ternary phase diagrams are not available. A partial phase diagram of Pb–Cr–O system and the Gibbs energy of formation of the all stable lead chromates were recently determined by the present authors [9,10]. This paper presents the results of the experiments carried out to establish the phase diagram of the ternary Pb–Fe–O system. The standard molar Gibbs energies of formation of two ternary oxygen compounds of these systems were also determined by measuring equilibrium oxygen pressures over appropriate ternary phase fields using solid oxide electrolyte based emf cells and are reported.

2. Literature review

Reaction between the oxides of lead and iron had been investigated in the past with a view to identify and characterize the compounds and to establish the pseudo binary $PbO–Fe_2O_3$ system [11–27]. The reactions between the oxides were observed to be very sluggish leading to the formation of several possible meta stable phases with uncertainties in their composition [16,23,25]. As many as eleven compounds with the following compositions have been reported in the past: $8PbO{\cdot}Fe_2O_3$, $3PbO{\cdot}Fe_2O_3$, $2PbO{\cdot}Fe_2O_3$, $3PbO{\cdot}2Fe_2O_3$, $PbO{\cdot}Fe_2O_3$, $PbO{\cdot}2Fe_2O_3$, $2PbO{\cdot}5Fe_2O_3$, $PbO{\cdot}3Fe_2O_3$, $PbO{\cdot}4Fe_2O_3$, $PbO{\cdot}5Fe_2O_3$, and $PbO{\cdot}6Fe_2O_3$. All the data reported in the literature are listed in Table 1.

Although the existence of $8PbO{\cdot}Fe_2O_3$, $3PbO{\cdot}Fe_2O_3$, $3PbO{\cdot}2Fe_2O_3$, $PbO{\cdot}Fe_2O_3$ and $PbO{\cdot}3Fe_2O_3$ had been reported in the early works [11,12,17–19,21], these compounds were not observed in the subsequent works reported in Refs. [22–27], indicating them to be meta stable. Among the other compounds, existence of $2PbO{\cdot}Fe_2O_3$, generally referred as δ phase, is reported by nearly all workers [13,14,16,19,21–27]. It is known to be stoichiometric,

* Corresponding author. Tel.: +91 44 2748 0302; fax: +91 44 2748 0065.
E-mail address: gnani@igcar.gov.in (T. Gnanasekaran).

0022-3115/$ - see front matter © 2012 Elsevier B.V. All rights reserved.
http://dx.doi.org/10.1016/j.jnucmat.2012.03.032

Table 1
Literature data on Pb–Fe–O system.

Sl. No	Authors	Experimental techniques	Identified compounds and Temperature range of stability
1	Kohlmeyer [11]	Thermogram and microscopy	$3PbO{\cdot}Fe_2O_3$, $3PbO{\cdot}2Fe_2O_3$, $PbO{\cdot}Fe_2O_3$, $PbO{\cdot}2Fe_2O_3$
2	Paramonov [12]	Heating of PbO and Fe_2O_3 at various temperatures and various time periods	$PbO{\cdot}Fe_2O_3$ (T: 938–998 K)
3	Cocco [13]	Microscopy and XRD	$2PbO{\cdot}Fe_2O_3$ (forms below 1113 K), $2PbO{\cdot}5Fe_2O_3$, $PbO{\cdot}5Fe_2O_3$
4.	Berger and Pawlek [14]	Mixtures of PbO and Fe_2O_3 at various compositions pelletized and heated. Phases were analyzed by XRD.	$2PbO{\cdot}Fe_2O_3$, $PbO{\cdot}2Fe_2O_3$, $PbO{\cdot}6Fe_2O_3$
5	Margulis and Kopylov [15]	Thermal analysis, microscopy, XRD of specified molar ratios of PbO to Fe_2O_3 .	$PbO{\cdot}4Fe_2O_3$ (Decomposes at 1413 K)
6	Mountvala and Ravitz [16]	Dry powders of PbO and Fe_2O_3 mixed and heated. Only PbO/Fe_2O_3 mole ratio 2 or less were studied by DTA and XRD	δ: $2PbO{\cdot}Fe_2O_3$ (T: ~923–1183 K) γ: $PbO{\cdot}(2\text{-}2.5)Fe_2O_3$ (T: 1023–1218 K) β: $PbO{\cdot}(5\text{-}6)Fe_2O_3$ (T: 1033–1588 K)
7	Cassadanne [18]	Compounds were prepared by coprecipitation of stoichiometric amount of mixtures of lead and iron in NaOH at pH 9. Samples were heated and analyzed by DTA and XRD.	$PbO{\cdot}3Fe_2O_3$, (T: 773–1443 K) $3PbO{\cdot}Fe_2O_3$ (stable below 1123 K) $8PbO{\cdot}Fe_2O_3$ (stable below 1013 K)
8	Jonker [20]	Mixtures of PbO and Fe_2O_3 were studied by DTA and liquidus temperatures were determined.	Liquidus curve on $PbO\text{-}(0\text{–}40\ mol\%)Fe_2O_3$ system
9	Mexmain and Hivert [21]	Mixtures of PbO and Fe_2O_3 of various compositions were studied by TG/DTA and XRD.	$2PbO{\cdot}Fe_2O_3$(T : stable up to 1143 K) $PbO{\cdot}3Fe_2O_3$ (T : stable up to 1184 K) $PbO{\cdot}6Fe_2O_3$ (T : stable up to 1348 K)
10	Shaaban et al. [22]	$PbO_2 + Fe_2O_3$ with different molar ratios (PbO_2:Fe_2O_3-19:1, 4:1, 1:1, 1:4), in air Max. Temp. 973 K TG, XRD	$2PbO{\cdot}Fe_2O_3$ (T: 703–1183 K) $PbO{\cdot}(2\text{-}2.5)Fe_2O_3$ (T: 683–1218 K) $PbO{\cdot}(4\text{-}6)Fe_2O_3$ (T: 933–1588 K)
11	Nevriva and Fischer [23]	Compound preparation by solution route, DTA for different compositions of PbO: Fe_2O_3. DTA, XRD	$PbO{\cdot}6Fe_2O_3$ $2PbO{\cdot}Fe_2O_3$ (stable up to 1143 K) $PbO{\cdot}(2+x)Fe_2O_3$ (stable up to 1153 K)
12	Raghavan [24]	Compilation up to 1989	$2PbO{\cdot}Fe_2O_3$ (T: ~923–1143 K) $PbO{\cdot}2Fe_2O_3$ (T: 1023–1153 K) $PbO{\cdot}(6-x)Fe_2O_3$ (T: 1073–1588 K)
13	Rivolier et al. [25]	Heating stoichiometric ratios of PbO and Fe_2O_3 powders. DTA with different mole % of Fe_2O_3 in 1 atm oxygen. TG/DTA, XRD	$2PbO{\cdot}Fe_2O_3$ (T: 973–1143 K) $PbO{\cdot}2.5Fe_2O_3$ (T: 973–1188 K) $PbO{\cdot}6Fe_2O_3$ (T: 973–1563 K)
14	Diop et al. [26, 27]	Annealing of stoichiometric mixtures of PbO and Fe_2O_3. TG/DTA, XRD, EPMA	$2PbO{\cdot}Fe_2O_3$ (T: 968–1133 K) $PbO{\cdot}2.5Fe_2O_3$ (T: 1043–1193 K) $PbO{\cdot}6Fe_2O_3$ (T: ~1083–1623 K)

but its temperature range of stability is not clearly established. Shaaban et al. [22] have reported that this compound can be formed by solid state reaction between Pb_3O_4 and Fe_2O_3 at 703 K itself while the reaction between PbO and Fe_2O_3 yields this compound only at 923 K.

The compounds with stoichiometries of $PbO{\cdot}2Fe_2O_3$ and $PbO{\cdot}2.5Fe_2O_3$ are reported in Refs. [16,22,23]. Their XRD patterns are given in JCPDS file 22–0656 and JCPDS file 49–0753 respectively. But these XRD patterns are identical with slight shifts in peak positions, suggesting that they correspond to a non-stoichiometric compound as observed by Mountvala and Ravitz [16] and Shaaban et al. [22]. Rivolier et al. [25] discussed this issue in detail and suggested it as a stoichiometric compound of composition $PbFe_5O_{8.5}$, although the authors could not completely rule out the non-stoichiometry in it. Shaaban et al. [22] have reported this compound as non-stoichiometric with the composition range of $PbO{\cdot}2Fe_2O_3$ to $PbO{\cdot}2.5\ Fe_2O_3$. This could be formed at 683 K itself by solid-state reaction between Pb_3O_4 and Fe_2O_3 while it was formed only above 973 K when PbO and Fe_2O_3 were the starting materials [16,23–27]. In the present paper, it is represented with a nominal composition of '$PbFe_5O_{8.5}$'.

Although the existence of compounds such as $PbO{\cdot}4Fe_2O_3$ [15], $PbO{\cdot}5Fe_2O_3$ [13] and $PbO{\cdot}6Fe_2O_3$ [14,21,23,25–27] have been reported, presence of non-stoichiometry in the ranges of $PbO{\cdot}4\text{-}6Fe_2O_3$ [22] as well as $PbO{\cdot}5\text{-}6Fe_2O_3$ [16,24] have also been reported. In the recent works [25–27], $PbO{\cdot}6Fe_2O_3$ is reported to be stoichiometric, but there is no substantial experimental evidence to rule out the non-stoichiometry in this compound also. However, there is a consensus that the composition of the iron oxide rich terminal of this non-stoichiometric compound is $PbO{\cdot}6Fe_2O_3$. In the present work, nominal composition of this compound is represented as '$PbFe_{12}O_{19}$'.

It is to be pointed out that no data on the ternary phase diagram of Pb–Fe–O system has been reported so far and no experimental data on the thermochemical properties of the three ternary oxides viz. $Pb_2Fe_2O_5$, '$PbFe_5O_{8.5}$' and '$PbFe_{12}O_{19}$' is available in literature.

3. Experimental

3.1. Materials

Fe_2O_3 powder (99.99% purity on metal basis, M/s Alfa Aesar, UK) and PbO powder (99.9 + % purity on metal basis, M/s Aldrich Chem. Co., USA) were used. Thermogravimetry experiments coupled with evolved gas analysis showed that PbO and Fe_2O_3 contained 1.37 wt% and 0.17 wt% of moisture, respectively. It was also found that PbO contained 2 wt% lead carbonate impurity. The PbO powder was therefore heated in argon atmosphere at 773 K for 2 h to convert the carbonate impurity into oxide and to remove moisture. The Fe_2O_3 powder was calcined in air at 523 K for 2 h to remove the moisture. Lead powder (99.9% purity, M/s Alfa Aesar, USA) and iron powder (99.9 + % purity, M/s Alfa Aesar, UK) were used for phase equilibration studies. Very fine powder of lead metal was also prepared by reducing the PbO powder under flowing hydrogen at 598 K for 2 h. The ternary compounds were prepared by the so-

lid-state reaction of mixtures of appropriate molar ratios of lead oxide and iron oxide powders. The mixtures were taken in the form of compacted pellets and heated in alumina crucibles in ambient air at chosen temperatures ranging from 998 K to 1073 K for extended periods of time varying from ~50 h to 220 h. During these heating cycles, the sample pellets were cooled to room temperature at least once and were crushed and powdered. The powdered samples were again pelletized and heating in air was continued before finally quenching them in ice cold water. In order to obtain phase pure compounds, co-precipitation method was also undertaken. For this, stoichiometric amounts of PbO and high purity iron powder (99.9 + % purity, M/s Alfa Aesar, UK) were first dissolved in minimum amount of nitric acid and the resultant nitrate solution was added to an excess amount of ammonium hydroxide solution. The precipitate formed was then filtered, dried, pelletized and heated in air at 1048 K for 24 h. The products obtained by all these methods of preparation were characterized by X-ray diffraction using Siemens D500 X-ray powder diffractometer with Cu Kα radiation and graphite monochromator.

3.2. Phase equilibration studies

To derive the ternary phase diagram of Pb–Fe–O system, compacts of samples with compositions corresponding to different possible phase fields were made. Mixtures from pure metals, oxides and ternary compounds with different overall compositions, were prepared by thorough grinding of the component phases. Pellets of these mixtures were equilibrated in low volume sealed containers to avoid any compositional changes. Equilibrations were carried out at six different chosen temperatures viz.848 K, 898 K, 948 K, 993 K, 1048 K and 1133 K. Equilibrations lasted for a minimum period of 480 h when the chosen temperatures were 1048 K and 1133 K. At other lower temperatures, the equilibration was carried out for 720 h. Initial equilibration experiments were carried out by placing the sample pellets in an alumina crucible which in turn was placed in a quartz tube and vacuum sealed. It was observed that the quartz tubes invariably got attacked and sometimes even cracked at the end of equilibration experiments. Presumably PbO in vapor phase led to severe attacks which also would have resulted in altering the stoichiometries of the samples. To avoid these effects, the sample pellet was placed inside a zirconia container which was in turn kept inside a one end closed bright annealed copper tube which was free of any oxide layers. The open end of the tube was then crimped and sealed inside an argon atmosphere glove box by TIG welding. Copper was chosen for this containment since the oxygen potential needed to form Cu_2O are much higher than the oxygen potentials of Pb–PbO and Fe–FeO/Fe–Fe_3O_4 couples. The sample inside the sealed copper tube was equilibrated by placing the tube in a quartz container under a flow of argon gas. At the end of every 240 h of equilibration at the chosen temperature, the copper tube was quenched in liquid nitrogen. The products were retrieved, thoroughly ground and characterized by XRD. The sample was once again pelletized and equilibration at the chosen temperature was continued. In all the experiments where Pb was one of the coexisting phase, it was found to have collected into a single globule at the end of the equilibration. Before using the sample for the next equilibration, the lead globule was removed and equal weight of lead powder (prepared by reduction of PbO) was added to maintain the over all composition. The compositions of samples used for these equilibrations are given in Tables 2a and 2b. It is to be noted that several of the samples of identical overall composition were made by starting from different component phases. At the end of equilibrations, the samples were retrieved and analyzed by XRD.

3.3. Emf measurements

The following two galvanic cells were constructed and studied:

Cell-I
Run-1: (−) Kanthal, Ir, $Pb_{0.25}Fe_{0.30}O_{0.45}$ | YSZ | (O_2, 101.325 kPa), Pt (+)
Run-2: (−) Kanthal, Ir, $Pb_{0.55}Fe_{0.18}O_{0.27}$ | YSZ | (O_2, 101.325 kPa), Pt (+)

Cell-II
Run-1: (−) Kanthal, Ir, $Pb_{0.54}Fe_{0.15}O_{0.31}$ | YSZ | (O_2, 101.325 kPa), Pt (+)
Run-2: (−) Kanthal, Ir, $Pb_{0.47}Fe_{0.18}O_{0.35}$ | YSZ | (O_2, 101.325 kPa), Pt (+)

The schematic of the experimental assembly of the galvanic cells is shown in Fig. 1. One end closed yttria stabilized zirconia (YSZ) solid electrolyte tube having a flat bottom (13 mm OD, 9 mm ID and 300 mm long), supplied by M/s Nikkato Corporation, Japan was used for constructing the galvanic cells. The reference electrode for the cell was prepared by applying a platinum paste (M/s Eltecks Corporation, India) over the inner bottom surface of the electrolyte tube and heating it at 1373 K for 2 h in air. This resulted in a uniform and porous platinum film over the electrolyte surface. A Pt

Table 2a
Results of phase equilibration studies in Pb–Fe–O system at 848, 898, 948, and 993 K.

Sl. No	Phases taken before equilibration	Overall composition of the sample	T (K)	Phases identified after equilibration for 720 h
1	Fe–PbO–Fe_2O_3	$Pb_{0.04}Fe_{0.38}O_{0.58}$	848	PbO–Fe_2O_3–Fe_3O_4
2	Pb–PbO–$Pb_2Fe_2O_5$	$Pb_{0.40}Fe_{0.15}O_{0.45}$	848	Pb–PbO–Fe_3O_4
3	Fe–PbO–Fe_2O_3	$Pb_{0.40}Fe_{0.15}O_{0.45}$	848	Pb–PbO–Fe_3O_4
4	Fe–PbO–Fe_2O_3	$Pb_{0.03}Fe_{0.45}O_{0.52}$	848	Pb–FeO–Fe_3O_4
5	Pb–Fe_2O_3–$Pb_2Fe_2O_5$	$Pb_{0.03}Fe_{0.45}O_{0.52}$	848	Pb–FeO–Fe_3O_4
6	Fe–PbO–Fe_2O_3	$Pb_{0.15}Fe_{0.55}O_{0.30}$	848	Pb–Fe–FeO
7	Fe–PbO–FeO	$Pb_{0.25}Fe_{0.30}O_{0.45}$	848	Pb–PbO–Fe_3O_4
8	Fe–PbO–$Pb_2Fe_2O_5$	$Pb_{0.33}Fe_{0.22}O_{0.45}$	848	Pb–PbO–Fe_3O_4
9	PbO–FeO–Fe_2O_3	$Pb_{0.18}Fe_{0.27}O_{0.55}$	848	PbO–Fe_2O_3–Fe_3O_4
10	Pb–PbO–FeO	$Pb_{0.25}Fe_{0.30}O_{0.45}$	898	Pb–PbO–Fe_3O_4
			948	Pb–Fe_3O_4–'$PbFe_5O_{8.5}$'
11	PbO–FeO–Fe_2O_3	$Pb_{0.10}Fe_{0.34}O_{0.56}$	898	Pb–PbO–Fe_3O_4
			948	Pb–Fe_3O_4–'$PbFe_5O_{8.5}$'
12	FeO–PbO–'$PbFe_5O_{8.5}$'	$Pb_{0.18}Fe_{0.27}O_{0.55}$	993	Pb–PbO–'$PbFe_5O_{8.5}$'
13	Fe–PbO–'$PbFe_5O_{8.5}$'	$Pb_{0.33}Fe_{0.22}O_{0.45}$	993	Pb–PbO–'$PbFe_5O_{8.5}$'

Table 2b
Results of phase equilibration studies in Pb–Fe–O system at 1048 and 1133 K.

Sl. No	Phases taken before equilibration	Overall composition of the sample	Phases identified after equilibration for 480 h
14	$FeO–Fe_2O_3–Pb_2Fe_2O_5$	$Pb_{0.04}Fe_{0.38}O_{0.58}$	$Fe_3O_4–PbFe_5O_{8.5}–PbFe_{12}O_{19}$
15	$Fe–PbO–Fe_2O_3$	$Pb_{0.04}Fe_{0.38}O_{0.58}$	$Fe_3O_4–PbFe_5O_{8.5}–PbFe_{12}O_{19}$
16	$Pb–PbO–Pb_2Fe_2O_5$	$Pb_{0.40}Fe_{0.15}O_{0.45}$	$Pb–PbO–Pb_2Fe_2O_5$[a]
17	$Fe–PbO–Fe_2O_3$	$Pb_{0.40}Fe_{0.15}O_{0.45}$	$Pb–PbO–Pb_2Fe_2O_5$[a]
18	$Fe–PbO–Fe_2O_3$	$Pb_{0.03}Fe_{0.45}O_{0.52}$	$Pb–FeO–Fe_3O_4$
19	$Pb–Fe_2O_3–Pb_2Fe_2O_5$	$Pb_{0.03}Fe_{0.45}O_{0.52}$	$Pb–FeO–Fe_3O_4$
20	$Pb–Fe–Fe_2O_3$	$Pb_{0.15}Fe_{0.55}O_{0.30}$	Pb–Fe–FeO
21	$Fe–PbO–Fe_2O_3$	$Pb_{0.15}Fe_{0.55}O_{0.30}$	Pb–Fe–FeO
22	$Fe–PbO–PbFe_5\ O_{8.5}$	$Pb_{0.25}Fe_{0.30}O_{0.45}$	$Pb–Fe_3O_4–PbFe_5O_{8.5}$
23	$FeO–PbO–PbFe_5O_{8.5}$	$Pb_{0.10}Fe_{0.34}O_{0.56}$	$Pb–Fe_3O_4–PbFe_5O_{8.5}$
24	$Fe–PbO–Pb_2Fe_2O_5$	$Pb_{0.33}Fe_{0.22}O_{0.45}$	$Fe_3O_4–PbFe_5O_{8.5}–Pb_2Fe_2O_5$
25	$FeO–PbO–PbFe_{12}O_{19}$	$Pb_{0.18}Fe_{0.27}O_{0.55}$	$Fe_3O_4–PbFe_5O_{8.5}–Pb_2Fe_2O_5$

[a] At 1133 K liquid phase is present.

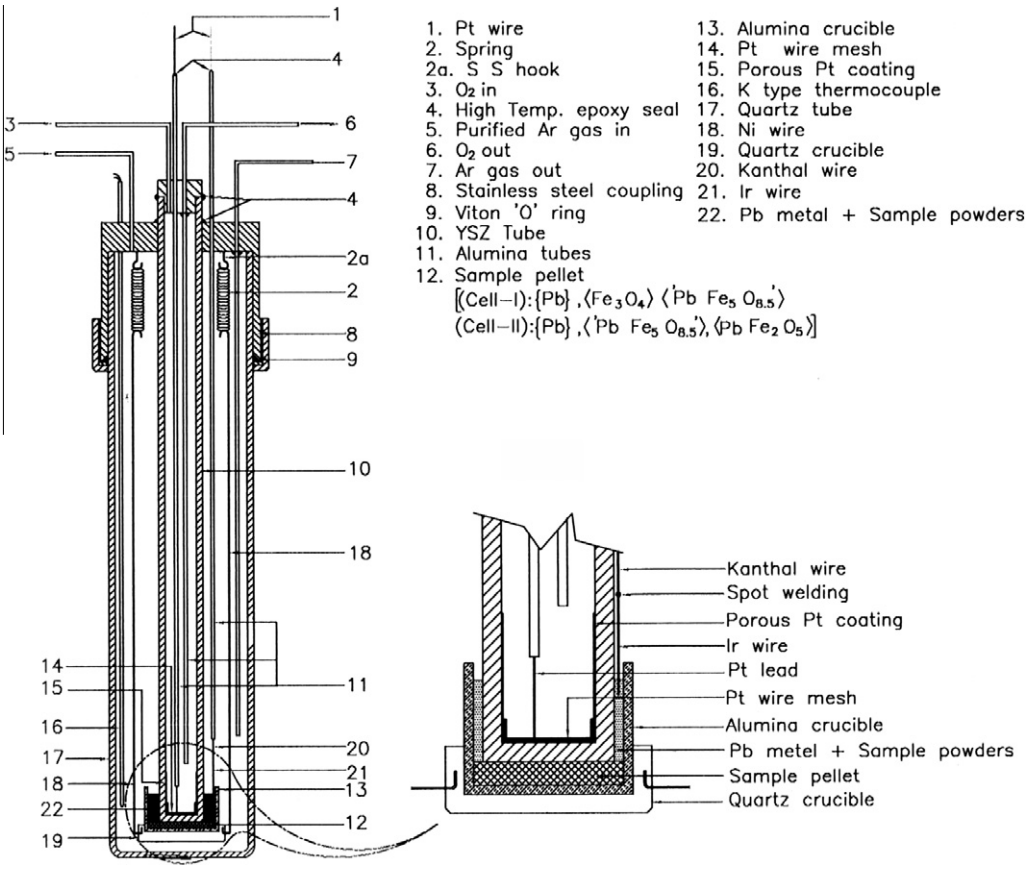

Fig. 1. Schematics of the solid oxide based galvanic cells used.

wire, co-fired with the platinum paste served as the electrical lead. A similar porous platinum electrode was also formed on the external surface at the bottom of the electrolyte tube. The performance of the emf cell was first tested by measuring the null emf as a function of temperature from 723 K to 1123 K by maintaining identical oxygen pressures on both sides of the electrolyte (air–air and oxygen–oxygen). Pt-electrode present at the external surface of the electrolyte tube was then removed, thoroughly cleaned and the electrolyte tube was used for measurements with sample electrodes. For both cells-I and II, same electrolyte tube was used. Two sample electrodes with different overall compositions but falling within the possible phase field of Pb(l)–Fe_3O_4–'$PbFe_5O_{8.5}$' were used for measurements with cell-I. In a similar manner, two sets of emf measurements were carried out with two different compositions falling in the possible phase field of Pb(l)–'$PbFe_5O_{8.5}$'–$Pb_2Fe_2O_5$.

The electrolyte tube was attached to a stainless steel coupling by means of a high temperature epoxy seal. A short iridium wire that dipped inside the sample electrode and spot welded to a Kanthal wire was used as the electrical lead in the sample side. For use as sample electrode, a mixture of oxide phases and lead metal powder was compacted to form a porous pellet of 12.5 mm dia and 1 to 2 mm thickness. This was placed at the bottom of an alumina crucible of 18 mm inner diameter and 20 mm height. The solid electrolyte tube was placed over this pellet. The volume around the electrolyte tube inside the crucible was filled with the phase field mixture. This ensured good contact between all the three phases and avoided the segrega-

tion of oxide phases from liquid lead due to the large differences in their densities. Alumina crucible containing the sample was placed over a quartz crucible. The quartz crucible had holes at the top of its circumference. A pair of kanthal wires connected to springs were attached through these holes and hung from the hooks provided in the inner surface of the stainless steel coupling. This arrangement ensured intimate contact between the electrolyte and sample electrode.

The sample-cum-electrolyte assembly was surrounded by a one end closed quartz tube which in turn was attached to the stainless steel coupling using an O-ring seal. The stainless steel coupling had provisions for placing a K-type thermocouple very close to the electrode–electrolyte assembly so that the cell temperature can be measured accurately. It also had provisions for flowing high purity argon and oxygen gases through the sample and reference compartments, respectively. High purity argon gas was obtained by passing commercial argon through a purification assembly. This assembly consisted of columns of regenerated LINDE 4A molecular sieves and active Cu impregnated $MgSiO_3$ pellets (popularly known as BASF catalyst) maintained at ambient temperature followed by three columns containing metallic copper turnings held at 773 K, titanium sponge held at 1173 K and calcium metal shots held at 773 K. The gas exiting from the outlet of the emf cell was again passed over another column containing calcium metal shots maintained at 773 K before letting it out to ambient air through an oil bubbler. The cell assembly was placed in the constant temperature zone of a furnace. Additionally, a 100 mm long and hollow cylindrical stainless steel block was placed in the constant temperature zone of the furnace to further enhance the uniformity of the temperature in the zone. Using this arrangement the cell temperature could be controlled within ±0.2 K using a PID temperature controller. The stainless steel block was grounded to avoid any a.c. pickup in the emf signal. The cell temperature was measured using the K-type thermocouple which was calibrated prior to actual experiments against a standard calibrated thermocouple supplied by National Physical Laboratory, India. The cell emf was measured using a high impedance electrometer (input impedance $>10^{14}\,\Omega$, M/s Keithley, USA, model-6514) and the temperature was recorded using a multimeter (M/s Agilent Technologies, Malaysia, model: 34970A Data acquisition/switch unit). An IBM PC using GPIB interface acquired the data every minute. At each temperature the readings were recorded when the cell emf was stable within ±0.05 mV for at least 6 h. Attainment of equilibrium was tested by passing a small amount of current through of the cell or by shorting the two electrical leads for a brief time and monitoring the cell output for restoration of the pre-test emf.

The measured cell emf was corrected for the thermo emf due to the dissimilar electrical leads viz., Kanthal–platinum by incorporating the data reported by Ganesan et al. [28]. As the junction between Kanthal and Ir was present in the constant temperature zone of the furnace along with the sensor head, the thermo emf due to Kanthal–Ir need not be considered. After the measurements, the sample electrodes were retrieved and analyzed by XRD.

4. Results and discussion

4.1. Preparation of ternary compounds

The temperature, duration of heating employed for preparing the compounds and the phases formed by the solid state reaction between the oxides and also through the solution route are given below:

4.1.1. Solid state reaction between oxides

$$2PbO + Fe_2O_3 \xrightarrow{998K,51h} Pb_2Fe_2O_5 \quad (a)$$

$$PbO + 6Fe_2O_3 \xrightarrow{1073K,220h} \text{`}PbFe_{12}O_{19}\text{'} + Fe_2O_3 \quad (b)$$

$$PbO + 2Fe_2O_3 \xrightarrow{1073K,132h} \text{mixture of } PbFe_4O_7, Pb_2Fe_2O_5 \text{ and } Fe_2O_3 \quad (c)$$

4.1.2. Reaction between precursors prepared through solution route

Stoichiometric ratios of lead and iron hydroxides were prepared by the dissolution of PbO and Fe powders in nitric acid followed by precipitation by addition of NH_4OH and were heated in air as follows:

$$Pb(OH)_2 + 4Fe(OH)_3 \xrightarrow{1048K,24h} \text{`}PbFe_5O_{8.5}\text{'} \quad (PbO : Fe_2O_3 = 1 : 2) \quad (d)$$

$$Pb(OH)_2 + 5Fe(OH)_3 \xrightarrow{1048K,24h} \text{`}PbFe_5O_{8.5}\text{'} \quad (PbO : Fe_2O_3 = 1 : 2.5) \quad (e)$$

$$Pb(OH)_2 + 6Fe(OH)_3 \xrightarrow{1048K,24h} \text{mixture of `}PbFe_5O_{8.5}\text{' and `}PbFe_{12}O_{19}\text{'} \quad (PbO : Fe_2O_3 = 1 : 3) \quad (f)$$

$$Pb(OH)_2 + 7Fe(OH)_3 \xrightarrow{1048K,24h} \text{mixture of `}PbFe_5O_{8.5}\text{' and `}PbFe_{12}O_{19}\text{'} \quad (PbO : Fe_2O_3 = 1 : 3.5) \quad (g)$$

$$Pb(OH)_2 + 8Fe(OH)_3 \xrightarrow{1048K,24h} \text{`}PbFe_{12}O_{19}\text{'} \quad (PbO : Fe_2O_3 = 1 : 4) \quad (h)$$

$$Pb(OH)_2 + 12Fe(OH)_3 \xrightarrow{1048K,24h} \text{`}PbFe_{12}O_{19}\text{'} \quad (PbO : Fe_2O_3 = 1 : 6) \quad (i)$$

XRD pattern of the product of reaction (a) matched with the pattern reported in JCPDS file 33–0756 confirming the phase purity of $Pb_2Fe_2O_5$. Attempts to prepare '$PbFe_{12}O_{19}$' by the solid-state reaction between PbO and Fe_2O_3 taken in the mole ratio of 1:6 (reaction b) always resulted in compound formation along with some unreacted Fe_2O_3. This could be because of the low reactivity of commercially procured sintered Fe_2O_3 used for these reactions and loss of PbO due to heating at 1073 K in air for 220 h (vapor pressure = 0.2 kPa at 1073 K). However, the XRD patterns of the products obtained through solution routes with mole ratios of PbO and Fe_2O_3 varying between 1:4 and 1:6, as shown by reaction (h) and (i), matched with that of the pattern reported for '$PbFe_{12}O_{19}$' in JCPDS file 41–1373. When preparations were carried out by heating the hydroxides with the ratios of PbO:Fe_2O_3 corresponding to 1:3 and 1:3.5, the products obtained were mixtures of '$PbFe_5O_{8.5}$' and '$PbFe_{12}O_{19}$'. These observations support the literature data on the non-stoichiometry of '$PbFe_{12}O_{19}$' (ranging from $PbO{\cdot}4Fe_2O_3$ to $PbO{\cdot}6Fe_2O_3$). Similarly, phase pure product of $PbFe_4O_7$, could not be obtained by the solid-state reaction between of PbO and Fe_2O_3 when taken in the mole ratio of 1:2 (reaction-c). However, the XRD patterns of products obtained through solution route with the mole ratios of PbO and Fe_2O_3 corresponding to 1:2 and 1:2.5 (reactions 'd' and 'e') matched with that of '$PbFe_5O_{8.5}$' reported in JCPDS file 49–0753 [25]. These results again indicate the

sluggishness of the direct solid state reactions between the oxides and the non-stoichiometry of '$PbFe_5O_{8.5}$' (ranging from $PbO{\cdot}2Fe_2O_3$ to $PbO{\cdot}2.5Fe_2O_3$).

4.2. Phase equilibration studies

Tables 2a and 2b summarize the results of long term equilibration studies carried out at the six temperatures chosen along with the composition of samples taken. Since the melting temperatures of the ternary compounds ($Pb_2Fe_2O_5$: 1143 K, '$PbFe_5O_{8.5}$': 1153 K, and for '$PbFe_{12}O_{19}$': 1588 K) involved are close to the equilibration temperatures, achievement of equilibrium is expected after the prolonged heating periods. This has been confirmed by the formation of products at the end of 240 h equilibrations itself. This is also shown by the formation of the equilibrium phases when different set of initial phases with same overall compositions were taken for long term equilibrations.

From the results indicated in Table 2a, the existence of the following phase fields could be identified at 848 K: (1) Pb–Fe–FeO, (2) Pb–FeO–Fe_3O_4, (3) Pb–PbO–Fe_3O_4 and (4) PbO–Fe_3O_4–Fe_2O_3. The results of experiments carried out at 898 K show that the Pb–PbO–Fe_3O_4 phase field exists at this temperature also. The results also show that the Pb–PbO–'$PbFe_5O_{8.5}$' phase field exists at 948 K, indicating that the ternary compound '$PbFe_5O_{8.5}$' appears as an equilibrium phase at a temperature between 898 and 948 K. The results shown in Table 2b indicate the existence of the following phase fields at 1048 K as well as at 1133 K: (1) Pb–Fe–FeO, (2) Pb–FeO–Fe_3O_4, (3) Fe_3O_4–Fe_2O_3–'$PbFe_{12}O_{19}$', (4) Fe_3O_4–'$PbFe_{12}O_{19}$' –'$PbFe_5O_{8.5}$', (5) Pb–Fe_3O_4–'$PbFe_5O_{8.5}$', (6) Pb–'$PbFe_5O_{8.5}$'–$Pb_2Fe_2O_5$ and (7) Pb–PbO–$Pb_2Fe_2O_5$. The existence of the phase field Pb–'$PbFe_5O_{8.5}$'–$Pb_2Fe_2O_5$ at 1048 K and above, indicates that $Pb_2Fe_2O_5$ appears as an equilibrium phase in the Pb–Fe–O system at a temperature between 948 and 1048 K. The temperatures above which the new ternary phases appear in this system were determined from the measurement of the equilibrium oxygen potentials using high temperature emf cells.

Table 3
Variation of emf of cell-I and deduced equilibrium oxygen potentials with temperature.

T (K)	E (mV)	$\Delta\overline{G}^{sple}_{O_2}$ / J mol^{-1}
Run 1		
1044.7	606.0	−233879.6
1069.6	593.8	−229171.2
1095.7	590.2	−227781.8
1110.4	584.9	−225736.3
1080.5	594.1	−229287.0
1065.5	599.0	−231178.1
1050.6	603.9	−233069.2
1035.9	609.1	−235076.1
1055.4	601.9	−232297.3
966.1	642.3	−247889.3
995.9	632.5	−244107.0
1005.8	627.9	−242331.7
981.1	639.9	−246963.0
1115.1	581.8	−224539.9
1101.3	586.5	−226353.8
1030.6	611.0	−235809.3
1041.6	611.1	−235847.9
1059.6	604.2	−233184.9
1025.6	619.2	−238974.0
1048.5	609.9	−235384.8
1085.1	594.6	−229479.9
1069.2	601.5	−232142.9
1015.5	622.4	−240209.1
951.0	648.5	−250282.1
935.6	655.7	−253060.9
945.4	651.4	−251401.3
1084.0	594.5	−229441.3
924.8	659.5	−254527.4
916.8	661.6	−255337.9
Run 2		
1092.3	583.0	−225003.0
1107.2	580.3	−223961.0
1077.7	590.8	−228013.4
1062.9	596.1	−230058.8
1048.4	601.6	−232181.5
1117.4	578.3	−223189.1
1033.7	612.3	−236311.1
1071.4	595.6	−229865.9
975.1	636.1	−245496.4
1088.1	588.7	−227202.9
1053.5	601.4	−232104.3
1045.2	604.0	−233107.8
1102.3	584.7	−225659.1
1057.9	600.4	−231718.4

Run 1: measurements with samples of overall composition $Pb_{0.25}Fe_{0.30}O_{0.45}$.
Run 2: measurements with samples of overall composition $Pb_{0.55}Fe_{0.18}O_{0.27}$.

4.3. EMF measurements

The time taken to reach equilibrium and stable emf values was in the range of 10–15 h at high temperatures, whereas this time exceeded 50 h at low temperatures and hence emf measurements could not be carried out below 917 K.

After completion of emf measurements involving several heating and cooling cycles, cell was cooled down to room temperature at 2 K/min, to avoid cracking of the solid electrolyte tube due to its poor thermal shock resistance. The samples were retrieved and analyzed by XRD which showed the presence of Pb–PbO–Fe_3O_4 along with some ternary compounds corresponding to high temperature phase fields which decomposed to give PbO and Fe_3O_4 on cooling. However, because of slow kinetics the decomposition was not complete.

EMF values of cell-I measured as a function of temperature is given in Table 3. The oxygen potential of sample, $\Delta\overline{G}^{sple}_{O_2}$, and that of the reference electrode, and $\Delta\overline{G}^{ref}_{O_2}$, are related to the cell emf as given below:

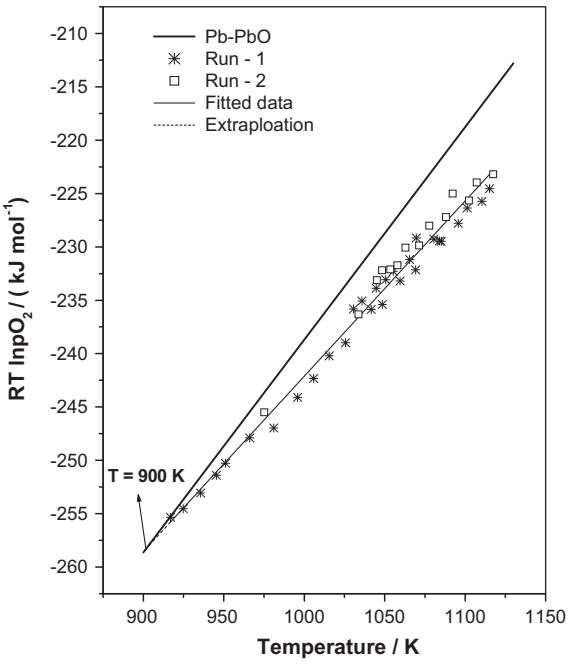

Fig. 2. Temperature dependence of equilibrium oxygen potentials of samples used in cell-I and those of Pb(l)–PbO(s) system.

$$4FE = RT\ln P_{O_2}^{ref} - RT\ln P_{O_2}^{sple} = \Delta\overline{G}_{O_2}^{ref} - \Delta\overline{G}_{O_2}^{sple} \quad (1)$$

$$\Delta\overline{G}_{O_2}^{sple} = \Delta\overline{G}_{O_2}^{ref} - 4FE,$$

$$\Delta\overline{G}_{O_2}^{sple} = -4FE, \text{since } P_{O_2}^{ref} = 1, \Delta\overline{G}_{O_2}^{ref} = 0 \quad (2)$$

Using the emf data, $\Delta\overline{G}_{O_2}^{sple}$ values were calculated and are also shown in Table 3. The data can be represented by the following least squared fitted line:

$$\Delta\overline{G}_{O_2}^{sple} \pm 1.1(\text{kJ mol}^{-1}) = -406.5 + 0.1643(T/\text{K}) \quad (917 \leqslant T/\text{K} \leqslant 1117) \quad (3)$$

The error given is the standard deviation of the least squares fitted line.

The measured oxygen potentials are shown in Fig. 2 and are compared with the oxygen potentials of Pb–PbO system deduced from the Gibbs energy of formation of PbO(s) [29]:

$$\Delta_f G_m^o\langle\beta - \text{PbO}\rangle \pm 0.10(\text{kJ mol}^{-1}) = -218.98 + 0.09963(T/\text{K}) \quad (612 \leqslant T/\text{K} \leqslant 1111) \quad (4)$$

$$\Delta\overline{G}_{O_2}^{Pb-PbO} \pm 0.20(\text{kJ mol}^{-1}) = 2\Delta_f G_m^o\langle\beta - \text{PbO}\rangle \quad (5)$$

Table 4
Variation of emf of cell –II and deduced equilibrium oxygen potentials with temperature.

T (K)	E (mV)	$\Delta\overline{G}_{O_2}^{sple}$/J mol^{-1}
Run 1		
1053.6	596.8	−230329.0
1080.7	585.4	−225929.3
1130.6	569.4	−219754.2
1029.5	606.3	−233995.4
1120.4	573.4	−221298.0
1041.7	599.5	−231371.0
1061.8	592.4	−228630.9
1095.4	580.8	−224154.0
1049.7	596.4	−230174.6
1100.2	579.5	−223652.2
1071.0	589.4	−227473.0
1090.9	583.1	−225041.6
1060.4	593.5	−229055.4
1125.4	573.0	−221143.6
1087.5	585.5	−225967.9
1117.0	576.7	−222571.6
1059.1	595.5	−229827.3
1035.6	603.7	−232992.0
1046.8	599.2	−231255.2
1125.7	572.1	−220796.3
1116.5	576.5	−222494.4
Run 2		
1068.5	591.9	−228437.9
1123.3	572.0	−220757.7
1086.8	584.4	−225543.3
1105.7	578.0	−223073.3
1057.0	595.3	−229750.1
1116.1	576.1	−222340.0
1079.5	588.4	−227087.1
1042.4	601.6	−232181.5
1019.6	611.4	−235963.7
984.0	628.4	−242524.7
962.1	638.1	−246268.3
949.1	643.3	−248275.2
1002.8	619.1	−238935.5
1097.3	582.1	−224655.7
1074.4	589.7	−227588.8
1052.0	597.9	−230753.5
1102.3	580.2	−223922.4
920.4	655.8	−253099.5
975.9	630.8	−243451.0

Run 1: measurements with samples of overall composition $Pb_{0.54}Fe_{0.15}O_{0.31}$.
Run 2: measurements with samples of overall composition $Pb_{0.47}Fe_{0.18}O_{0.35}$.

Extrapolation of the line representing $\Delta\overline{G}_{O_2}^{sple}$ versus temperature intersects the line corresponding to oxygen potential of Pb-PbO system at 900 K indicating the decomposition of '$PbFe_5O_{8.5}$' to PbO and Fe_3O_4 occurs below this temperature. This is also in agreement with the results of the phase equilibration studies discussed in Section 4.2.

The chemical equilibrium at the sample electrode is represented as below:

$$\text{Pb(l)} + 5/3\,\text{Fe}_3\text{O}_4\text{(s)} + 11/12\text{O}_2\,\text{(g)} \Longleftrightarrow \text{'PbFe}_5\text{O}_{8.5}\text{'(s)}$$

$$\Delta_f G_m^o\text{'PbFe}_5\text{O}_{8.5}\text{'} \Longleftrightarrow 5/3\,\Delta_f G_m^0\text{Fe}_3\text{O}_4 + 11/12\Delta\overline{G}_{O_2}^{sple} \quad (6)$$

By substituting $\Delta\overline{G}_{O_2}^{sple}$ given by Eq. (3) and by using the values $\Delta_f G_m^0 Fe_3O_4$ [30,31], the standard molar Gibbs energy of formation of '$PbFe_5O_{8.5}$' was derived and is given below:

$$\Delta_f G_m^0\text{'PbFe}_5\text{O}_{8.5}\text{'} \pm 1.0(\text{kJ mol}^{-1}) = -2208.1 + 0.6677(T/\text{K}) \quad (917 \leqslant T/\text{K} \leqslant 1117) \quad (7)$$

Emf values of cell-II obtained as a function of temperature are given in Table 4. The oxygen potential of the samples at each temperature of measurements, $\Delta\overline{G}_{O_2}^{sple}$, was deduced from emf data by using relations given by Eq. (2) and is given in Table 4. These data are plotted in Fig. 3 and compared with the oxygen potentials of Pb–PbO system. As seen from this Fig. 3, the measured oxygen potentials at temperatures below ~1030 K are in close agreement with the oxygen potentials of Pb–PbO system. This is also in agreement with the results of phase equilibration studies (Section 4.2) which showed that the phase fields Pb–PbO–$Pb_2Fe_2O_5$ and Pb–$Pb_2Fe_2O_5$–'$PbFe_5O_{8.5}$' exists only above a temperature falling between 948 K and 1048 K.

Equilibrium oxygen potentials of the sample measured above 1050 K were fitted to yield the following expression by the method of least squares:

$$\Delta\overline{G}_{O_2}^{sple} \pm 0.4(\text{kJ mol}^{-1}) = -366.0 + 0.1290(T/\text{K}) \quad (1050 \leqslant T/\text{K} \leqslant 1131) \quad (8)$$

Extrapolation of this line intersects the line corresponding to oxygen potentials of Pb–PbO system at 1024 K, the temperature at

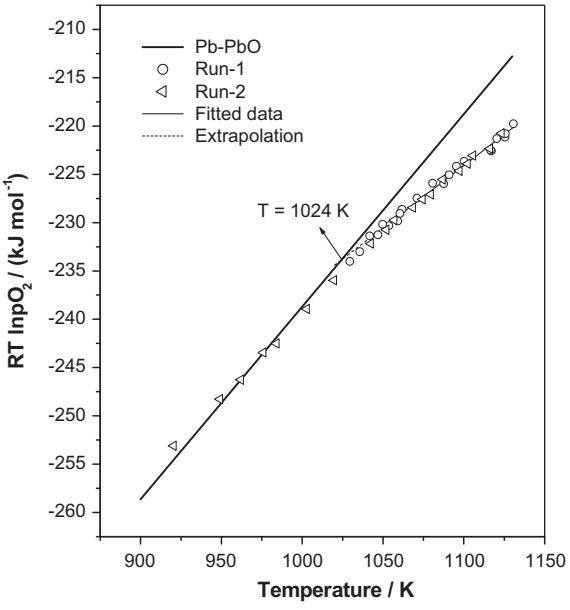

Fig. 3. Temperature dependence of equilibrium oxygen potentials of samples used in cell-II and those of Pb(l)–PbO(s) system.

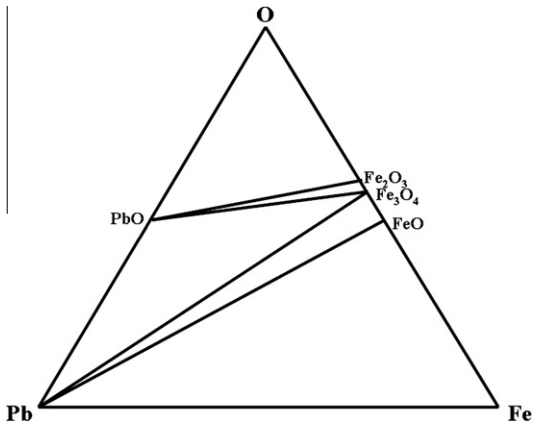

Fig. 4a. Partial phase diagram on Pb–Fe–O system from 848 K ⩽ T < 900 K.

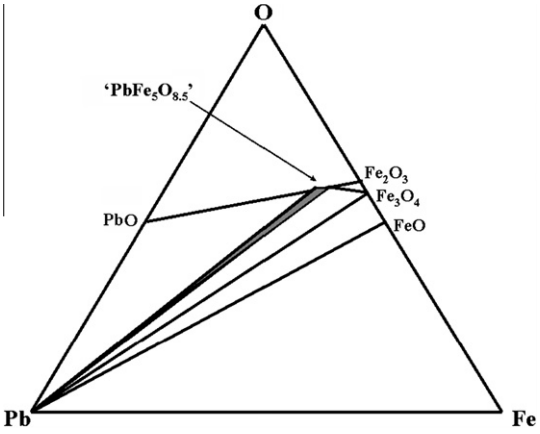

Fig. 4b. Partial phase diagram on Pb–Fe–O system from 900 K < T < 1024 K.

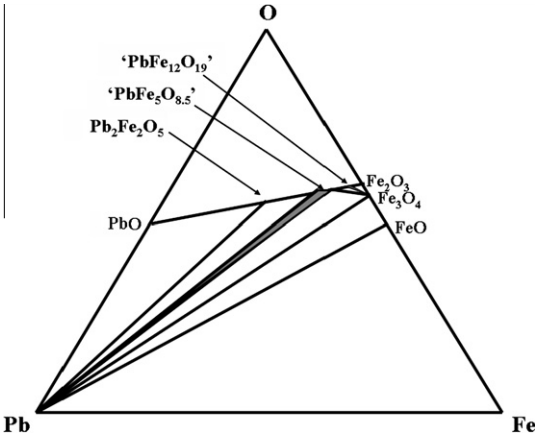

Fig. 4c. Partial phase diagram on Pb–Fe–O system from 1024 K < T ⩽ 1133 K.

which $Pb_2Fe_2O_5$ appears as an equilibrium phase in the ternary system.

Isothermal cross sections of the phase diagram of Pb–Fe–O system, taking into account of the appearance of '$PbFe_5O_{8.5}$' and $Pb_2Fe_2O_5$ as equilibrium phases at 900 K and 1024 K respectively, are constructed and shown in Figs. 4a–4c. Non-stoichiometry of '$PbFe_5O_{8.5}$' is indicated schematically in Figs. 4b and 4c.

It is to be pointed out that the temperatures at which '$PbFe_5O_{8.5}$' and $Pb_2Fe_2O_5$ appear as equilibrium phases based on present experimental results are different from those reported in Refs. [24,26].

The equilibrium reaction in cell-II at temperatures above 1050 K can be represented as below:

$$8/5\,\mathrm{Pb(l)} + 2/5\ \text{'}PbFe_5O_{8.5}\text{'(s)} + 4/5\ O_2(g) \Longleftrightarrow Pb_2Fe_2O_5(s) \quad (9)$$

$$\Delta_f G^o_m\langle Pb_2Fe_2O_5\rangle = \frac{4}{5}\Delta\overline{G}_{O_2} + \frac{2}{5}\Delta_f G^o_m\langle\text{'}PbFe_5O_{8.5}\text{'}\rangle \quad (10)$$

Gibbs energy of formation of $Pb_2Fe_2O_5$, $\Delta_f G^o_m\langle Pb_2Fe_2O_5\rangle$ can be deduced from the equilibrium oxygen potentials of cell-II and $\Delta_f G^o_m$'$PbFe_5O_{8.5}$'.

It is to be pointed out that the stoichiometry of '$PbFe_5O_{8.5}$' phase that exists in equilibrium during emf measurements in cell-I (Pb–'$PbFe_5O_{8.5}$'–Fe_3O_4) would be iron oxide rich. Gibbs energy of formation of '$PbFe_5O_{8.5}$' given by Eq. (7) corresponds to this iron oxide rich terminal composition. The composition '$PbFe_5O_{8.5}$' in the phase field of Pb–'$PbFe_5O_{8.5}$'–$Pb_2Fe_2O_5$ would be PbO rich. For deducing $\Delta_f G^o_m\langle Pb_2Fe_2O_5\rangle$ from Eq. (10), Gibbs energy of formation of PbO rich composition of '$PbFe_5O_{8.5}$' would be required. However, as shown in the Appendix, the change in compositions of '$PbFe_5O_{8.5}$' does not influence the deduced values of Gibbs energy of formation of $Pb_2Fe_2O_5$ significantly.

$\Delta_f G^o_m Pb_2Fe_2O_5$ deduced is given by the following expression:

$$\Delta_f G^o_m Pb_2Fe_2O_5 \pm 0.8(\mathrm{kJ\ mol^{-1}}) = -1178.4 + 0.3724(T/\mathrm{K}) \quad (1050 \leqslant T/\mathrm{K} \leqslant 1131) \quad (11)$$

Based on the data on Gibbs energies of formation of lead ferrates and lead chromates [9,10] and the available solubility data of oxygen in liquid lead, the nature of oxide layer in steel–liquid lead interface can be predicted. A detailed account on corrosion of steels in lead coolant circuits in light of thermochemical data of lead ferrates and lead chromates and also the composition of the steels used in them are discussed elsewhere [32].

5. Conclusion

The partial phase diagram of the ternary Pb–Fe–O system in the temperature range of 848–1133 K has been established for the first time.

(a) Temperature range of 1024–1133 K:
  (1) Pb–Fe–FeO, (2) Pb–FeO–Fe_3O_4, (3) Fe_3O_4–'$PbFe_{12}O_{19}$'–'$PbFe_5O_{8.5}$', (4) Pb–Fe_3O_4–'$PbFe_5O_{8.5}$', (5) Pb–'$PbFe_5O_{8.5}$'–$Pb_2Fe_2O_5$ and (6) Pb–PbO–$Pb_2Fe_2O_5$.

(b) Temperature range of 900–1024 K:
  (1) Pb–Fe–FeO, (2) Pb–FeO–Fe_3O_4, (3) Pb–Fe_3O_4–'$PbFe_5O_{8.5}$', and (4) Pb–PbO–'$PbFe_5O_{8.5}$'

(c) Temperature range of 848–900 K:
  (1) Pb–Fe–FeO, (2) Pb–FeO–Fe_3O_4, (3) Pb–PbO–Fe_3O_4, (4) PbO–Fe_3O_4–Fe_2O_3

Gibbs energy of formation of '$PbFe_5O_{8.5}$' and $Pb_2Fe_2O_5$ have been determined by measuring the equilibrium oxygen partial pressures in appropriate ternary phase fields using solid oxide electrolyte based emf cells. These thermochemical data are reported for the first time.

Acknowledgements

The authors acknowledge Dr. G. Panneerselvam, Dr. K.V.G. Kutty and his team for their help in recording XRD patterns of the samples. One of the authors (SKS) acknowledges Department of Atomic Energy, India for providing the financial support.

Appendix A

The equilibrium reaction in cell-II at temperatures above 1024 K can be represented as below:

$$8/5\,Pb(l) + 2/5\ 'PbFe_5O_{8.5}'(s) + 4/5\ O_2(g) \Longleftrightarrow Pb_2Fe_2O_5(s) \qquad (A)$$

Gibbs energy of formation of $Pb_2Fe_2O_5$, $\Delta_f G^o_m Pb_2Fe_2O_5$ can be deduced from the equilibrium oxygen potentials of cell-II and the $\Delta_f G^o_m$ '$PbFe_5O_{8.5}$' measured using cell-I. Since the non-stoichiometry in '$PbFe_5O_{8.5}$' ranges from $PbFe_4O_7$ ($PbO{\cdot}2Fe_2O_3$) to $PbFe_5O_{8.5}$ ($PbO{\cdot}2.5Fe_2O_3$), the influence of the variation of non-stoichiometry on the deduced values of Gibbs energy of formation of $Pb_2Fe_2O_5$ is considered as below.

A.1. By considering Fe_2O_3 rich end of non stoichiometry ($PbO{\cdot}2.5Fe_2O_3$) in equilibrium (A)

Gibbs energy of formation of $Pb_2Fe_2O_5$ can be deduced as,

$$\Delta_f G^o_m\langle Pb_2Fe_2O_5\rangle = \frac{4}{5}\Delta\overline{G}_{O_2} + \frac{2}{5}\Delta_f G^o_m\langle 'PbFe_5O_{8.5}'\rangle \qquad (B)$$

By incorporating the oxygen potentials of cell-II, $\Delta_f G^o_m\langle Pb_2Fe_2O_5\rangle$ is calculated as,

$$\Delta_f G^o_m\langle Pb_2Fe_2O_5\rangle(\text{kJ mol}^{-1}) = -1178.4 + 0.3724(T/\text{K}) \quad (1050 \leqslant T \leqslant 1131\text{K}) \qquad (C)$$

A.2. By considering PbO rich end of non stoichiometry ($PbO{\cdot}2Fe_2O_3$) in equilibrium (B)

The equilibrium at the sample electrode can be represented as below:

$$3/2\ Pb(l) + 1/2\ PbFe_4O_7(s) + 3/4\ O_2(g) = Pb_2Fe_2O_5(s) \qquad (D)$$

and the Gibbs energy of formation of $Pb_2Fe_2O_5$ can be given as

$$\Delta_f G^o_m\langle Pb_2Fe_2O_5\rangle = \frac{1}{2}\Delta_f G^o_m\langle PbFe_4O_7\rangle + \frac{3}{4}\Delta\overline{G}^{sple}_{O_2} \qquad (E)$$

Assuming ideal behavior for dissolution of Fe_2O_3 in $PbFe_4O_7$ to form the non-stoichiometry up to $PbFe_5O_{8.5}$, $\Delta_f G^0_m\langle PbFe_4O_7\rangle$ could be derived from $\Delta_f G^0_m$'$PbFe_5O_{8.5}$' as follows:

$$\Delta_m G^0_f\langle PbFe_4O_7\rangle = \Delta_m G^0_f\text{'}PbFe_5O_{8.5}\text{'} - 1/2\ \Delta_m G^0_f\langle Fe_2O_3\rangle - G^{mix} \qquad (F)$$

For ideal solution leading to formation of '$PbFe_5O_{8.5}$',

$$G^{mix} = -RT \sum_i X_i \ln X_i$$

Since $X_{Fe_2O_3}$ and $X_{PbFe_5O_{8.5}}$ in '$PbFe_5O_{8.5}$' are 2/3 and 1/3, $G^{mix} = -(5.292\times10^{-3})\,T$.

By substituting the value of G^{mix}, $\Delta_m G^0_f$ '$PbFe_5O_{8.5}$' from Eq. (7) and $\Delta_m G^0_f\langle Fe_2O_3\rangle$ [30,31], $\Delta_m G^0_f\langle PbFe_4O_7\rangle$ could be derived as,

$$\Delta_m G^0_f\langle PbFe_4O_7\rangle(\text{kJ mol}^{-1}) = -1800.7 + 0.5467(T/\text{K}) \quad (917 \leqslant T \leqslant 1117\text{K}) \qquad (G)$$

By incorporating the value of $\Delta_m G^0_f\langle PbFe_4O_7\rangle$ from (G) in Eq. (E), $\Delta_m G^0_f\langle Pb_2Fe_2O_5\rangle$ is obtained as

Table 5
Gibbs energy of formation of $Pb_2Fe_2O_5$, $\Delta_m G^0_f\langle Pb_2Fe_2O_5\rangle$, kJ mol^{-1}.

T (K)	From Eq. (C)	From Eq. (H)	% Of difference in data obtained through approaches A and B
1050	−787.4	−786.4	0.13
1100	−768.8	−767.8	0.13
1130	−757.6	−756.6	0.13

$$\Delta_m G^0_f\langle Pb_2Fe_2O_5\rangle(\text{kJ mol}^{-1}) = -1177.1 + 0.3721(T/\text{K}) \quad (1050 \leqslant T \leqslant 1131\text{K}) \qquad (H)$$

Values of $\Delta_m G^0_f\langle Pb_2Fe_2O_5\rangle$ deduced from Eqs. (C) and (H) are shown in Table 5. It is seen that the influence of neglecting the non-stoichiometry for deducing Gibbs energy of formation of $Pb_2Fe_2O_5$ is very small.

References

[1] B.F. Gromov (Ed.), Proceedings of Heavy Liquid Metal Coolants in Nuclear Technology HLMC 98, vols. 1 and 2, SSC RF-IPPE, Obninsk, 1999.
[2] B.F. Gromov, Y.I. Orlov, P.N. Martynov, V.A. Gulevsky, in: Proceedings of Heavy Liquid Metal Coolants in Nuclear Technology (HLMC-98), Vol. 1, Obninsk, 1998, pp. 87–91.
[3] P.N. Martynov, Y.I. Orlov, in: Proceedings of Heavy Liquid Metal Coolants in Nuclear Technology (HLMC-98), vol. 2, Obninsk, 1998, pp. 565–576.
[4] V.A. Gulevsky, P.N. Martynov, Y.I. Orlov, M.E. Chemov, in: Proceedings of Heavy Liquid Metal Coolants in Nuclear Technology (HLMC-98), vol. 2, Obninsk, 1998, pp. 668–677.
[5] N. Li, J. Nucl. Mater. 300 (2002) 73–81.
[6] G. Müller, A. Heinzel, G. Schumacher, A. Weisenburger, J. Nucl. Mater. 321 (2003) 256–262.
[7] T. Tsuji, K. Tsumura, K. Naito, J. Nucl. Mater. 138 (1986) 215–221.
[8] T. Horita, Y. Xiong, K. Yamaji, H. Kishimoto, N. Sakai, M.E. Brito, H. Yokokawa, Solid State Ion. 174 (2004) 41–48.
[9] S.K. Sahu, R. Ganesan, T. Gnanasekaran, J. Nucl. Mater. 376 (2008) 366–370.
[10] S.K. Sahu, R. Ganesan, T. Gnanasekaran, J. Chem. Thermodyn. 42 (2010) 1–7.
[11] E.J. Kohlmeyer, J. Metall Erz Metal. Erz. 10 (1913) 483–489.
[12] L.I. Paramonov, Tzvetnuie Metal. (1934) 79–88.
[13] A. Cocco, Ann. Chim. (Rome) 45 (1955) 737–753.
[14] W. Berger, F. Pawlek, Arch. Eisenhuettenwes. 28 (1957) 101–108.
[15] E.V. Margulis, N.I. Kopylov, Russ. J. Inorg. Chem. 5 (1960) 1196–1199.
[16] A.J. Mountvala, S.F. Ravitz, J. Am. Ceram. Soc. 45 (1962) 285–288.
[17] D.M. Chizhikov, T.E. Konvshkova, Akademii Nauk SSSR 12 (1963) 72–78.
[18] J. Cassedanne, Anais. Acad. Bras. Cienc. 36 (1964) 417–422.
[19] V.E. Rudnichenko, B.L. Dobrotsvetov, D.M. Kheiker, Tsvetn. Metal. 23 (1965) 389–399.
[20] H.D. Jonker, J. Crystal Growth 28 (1975) 231–239.
[21] J. Mexmain, S.-L. Hivert, Ann. Chim. Fr. 3 (1978) 91–97.
[22] S.A. Shaaban, M.F. Abadir, A.N. Mahdy, Trans. J. Br. Ceram. Trans. 83 (1984) 102–105.
[23] M. Nevriva, K. Fischer, Mater. Res. Bull. 21 (1986) 1285–1290.
[24] V. Raghavan (Ed.), Phase Diagram of Ternary Iron Alloys, Part 5, Ternary System Containing Iron and Oxygen, The Indian Institute of Metals, Calcutta, 1989, pp. 242–244.
[25] J.L. Rivolier, M. Ferriol, R. Abraham, M.T. Cohen-Adad, Eur. J. Solid State Inorg. Chem. 30 (1993) 727–739.
[26] I. Diop, N. David, J.M. Fiorani, R. Podor, M. Vilasi, Mater. Sci. Forum 595–598 (2008) 473–481.
[27] I. Diop, N. David, J.M. Fiorani, R. Podor, M. Vilasi, Thermochim. Acta 510 (2010) 202–212.
[28] R. Ganesan, T. Gnanasekaran, R.S. Srinivasa, J. Nucl. Mater. 375 (2008) 229–242.
[29] R. Ganesan, T. Gnanasekaran, R.S. Srinivasa, J. Nucl. Mater. 320 (2003) 258–264.
[30] B. Sundman, J. Phase Equilib. 12 (1991) 127–140.
[31] A.T. Dinsdale, Calphad 15 (1991) 317–425.
[32] A.V. Meera, S.K. Sahu, R. Ganesan, T. Gnanasekaran, Corrosion Science (communicated).